

Range Identification for Perspective Dynamic Systems with 3D Imaging Surfaces

Lili Ma, *Student Member, IEEE*, YangQuan Chen and Kevin L. Moore, *Senior Members, IEEE*

Center for Self-Organizing and Intelligent Systems (CSOIS),
 Dept. of Electrical and Computer Engineering, 4160 Old Main Hill,
 Utah State University (USU), Logan, UT 84322-4160, USA.

Abstract—Range identification using image sequence via observations from a traditional camera-type vision system has been discussed in the literature. In this paper, the camera-type planar imaging surface is extended to several well-known 3D surfaces, such as an arbitrary plane, a sphere, an ellipsoid, and a paraboloid. For a general imaging surface, the resulting perspective dynamic system is not guaranteed to preserve an affine form. In this case, most existing nonlinear observers that are applicable to the perspective dynamic system observed via a camera can not be applied for the range identification problem directly. We show via simulations that our recently proposed linear approximation observer can perform the state estimation.

Key Words: Perspective dynamic system, 3D imaging surface, range identification, nonlinear observer.

I. INTRODUCTION

Conventional video cameras have limited fields of view that make them restrictive in a variety of vision applications, including autonomous navigation, video conferencing, and scene recovery. Existing devices typically use a photographic camera or a video camera, in conjunction with an off-the-shelf lens. This configuration allows the device to view the world through a relatively small solid angle subtended from the center of projection of the lens. To enhance the field of view (FOV), omnidirectional/panoramic imaging sensors that have big, close to hemi-spherical FOV are under developments [1]. It is desirable that the entire imaging system still possesses a single effective viewpoint to enable the generation of pure perspective images [2]. In this way, available works in computational vision that assume linear perspective projection can be applied for processing [3].

Current technologies to achieve wide FOV are illustrated in Table I, where each technology is briefly listed in the followings [4]:

- 1) Rotating camera: it requires moving parts and precise positioning. A drawback lies in the total time to obtain an image with enhanced FOV.

Corresponding author: Prof. YangQuan Chen, Center for Self-Organizing and Intelligent Systems, Dept. of Electrical and Computer Engineering, 4160 Old Main Hill, Utah State University, Logan, UT 84322-4160. E: yqchen@ece.usu.edu, T: (435)7970148, F: (435)7973054, W: www.csois.usu.edu

K. L. Moore is now with the Research and Technology Development Center, Johns Hopkins University Applied Physics Laboratory, 11100 Johns Hopkins Road, Laurel, MD 20723-6099, E-mail: kevin.moore@jhuapl.edu

- 2) Cluster of cameras: centers of projections reside inside each individual camera. Consequently, the entire imaging system does not have a unique effective viewpoint.
- 3) Fish-eye lens: it is difficult to design a fish-eye lens that ensures that all the incoming rays intersect at a single point to yield a fixed viewpoint. Using two fish-eye lens that each provides a hemi-spherical FOV requires perfect seaming.
- 4) Catadioptric camera: incorporate reflecting surfaces (mirrors) into conventional imaging systems.

Though different difficulties exist in the above categorized technologies to construct powerful omnidirectional imaging systems, it is clear that imaging systems are not restricted to the camera-type vision system. While efforts are being carried on towards the construction of different candidates of omnidirectional vision systems, in this paper, we disregard the physical construction issue, but focus on the range identification problem via observations on a sphere, an ellipsoid, and a paraboloid. Our discussion of the range identification problem is based on the the perspective dynamic system (PDS) framework [5], [6], [7], [8], [9], [10], [11], [12], [13], [14]. Further, we assume that the discussed omnidirectional systems have a single center of projection such that the images observed preserve linear perspective geometry. Parameters of the imaging surface are also assumed known.

In a PDS system, the projection of a 3D point $[X, Y, Z]^T$ can only be observed up to a homogeneous line. That is

$$X_p = Z_p X/Z, \quad Y_p = Z_p Y/Z, \quad (1)$$

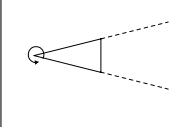
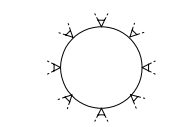
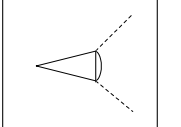
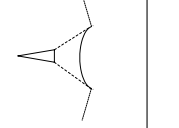
where the subscript_p denotes the projection on the imaging surfaces. In a setup with a stationary sensing system and a moving object, where the object follows an affine motion described by

$$\begin{bmatrix} \dot{X}(t) \\ \dot{Y}(t) \\ \dot{Z}(t) \end{bmatrix} = \begin{bmatrix} a_{11} & a_{12} & a_{13} \\ a_{21} & a_{22} & a_{23} \\ a_{31} & a_{32} & a_{33} \end{bmatrix} \begin{bmatrix} X(t) \\ Y(t) \\ Z(t) \end{bmatrix} + \begin{bmatrix} b_1 \\ b_2 \\ b_3 \end{bmatrix}, \quad (2)$$

two important issues in the PDS include:

- 1) Range identification problem: assuming that the motion parameters $a_{i,j}$ and b_i for $i, j = 1, 2, 3$ are known, to estimate the position of an object with unknown initial condition from observations on the imaging surface [12], [13], [14].

TABLE I
TECHNOLOGIES TO ACHIEVE WIDE FIELDS OF VIEW

Rotating Camera	Cluster of Cameras	Fish-eye Lens	Catadioptric Lens
			

- 2) Identification of motion parameters: assuming that the motion parameters $a_{i,j}$ and b_i for $i, j = 1, 2, 3$ are unknown, to identify the motion parameters to the extent possible from observations on the imaging surface [5], [6], [7], [8], [9], [10], [11].

The above two problems, especially the first one, will be discussed in this paper with general 3D imaging surfaces.

The paper is organized as follows. In Sections II and III, we document the PDS equations with general planar and ball-shape surfaces, where the PDS equations preserve affine forms. Section IV addresses the same problem via observations on a paraboloid. The resulting PDS no longer holds an affine form such that most of the existing perspective observers can not be applied for the range identification directly. Simulation results are presented in Sec. V to show that our recently proposed linear approximation-based observer (LAO) can perform the task even with nontraditional imaging surfaces. Finally, Sec. VI concludes the paper.

II. PDS WITH GENERAL PLANAR IMAGING SURFACE

An arbitrary planar surface, as shown in Fig. 1, can be described by its normal vector $\vec{n} = [n_1, n_2, n_3]^T$ and a point on the plane. To simplify derivations, the point on the plane is chosen to be $[0, 0, 1]^T$ without loss of generality. Thus, for any point $[X_p, Y_p, Z_p]^T$ on the plane, we have

$$n_1 X_p + n_2 Y_p + n_3 (Z_p - 1) = 0, \quad (3)$$

where we further assume $n_3 \neq 0$ to enforce the imaging surface facing toward the Z axis. From equations (1) and (3), we can write

$$X_p = n_3 X / \mathcal{L}_{pl}, \quad Y_p = n_3 Y / \mathcal{L}_{pl}, \quad Z_p = n_3 Z / \mathcal{L}_{pl}, \quad (4)$$

where $\mathcal{L}_{pl} \triangleq n_1 X + n_2 Y + n_3 Z$ and the subscript_{pl} denotes the *planar* surface.

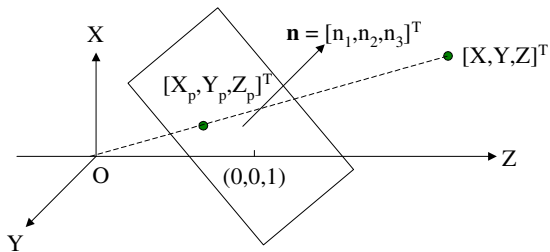


Fig. 1. A general planar imaging surface passing through $[0, 0, 1]^T$ with normal vector $\vec{n} = [n_1, n_2, n_3]^T$.

Since n_3 is known (parameters of the imaging surface are assumed known in this paper), we can choose $y(t) = [y_1, y_2, y_3]^T$ with

$$y_1 = X / \mathcal{L}_{pl}, \quad y_2 = Y / \mathcal{L}_{pl}, \quad y_3 = 1 / \mathcal{L}_{pl}, \quad (5)$$

where (y_1, y_2) are measurable from the imaging surface and y_3 contains the range information to estimate. From the above equation, $[X, Y, Z]^T$ can be calculated as:

$$X = \frac{y_1}{y_3}, \quad Y = \frac{y_2}{y_3}, \quad Z = \frac{1 - n_1 y_1 - n_2 y_2}{n_3 y_3}. \quad (6)$$

Under the choice of $y(t)$ as in (5) and the assumption that the object is moving according to the affine motion described by (2), the derivative of $y(t)$ is:

$$\begin{cases} \begin{bmatrix} \dot{y}_1 \\ \dot{y}_2 \end{bmatrix} = \begin{bmatrix} \frac{a_{13}}{n_3} + (a_{11} - a_{13} \frac{n_1}{n_3} - \rho_3) y_1 + (a_{12} - a_{13} \frac{n_2}{n_3}) y_2 \\ \frac{a_{23}}{n_3} + (a_{21} - a_{23} \frac{n_1}{n_3}) y_1 + (a_{22} - a_{23} \frac{n_2}{n_3} - \rho_3) y_2 \end{bmatrix} \\ \quad + \begin{bmatrix} -\rho_1 y_1^2 - \rho_2 y_1 y_2 \\ -\rho_1 y_1 y_2 - \rho_2 y_2^2 \end{bmatrix} + \begin{bmatrix} b_1 - \rho_0 y_1 \\ b_2 - \rho_0 y_2 \end{bmatrix} y_3, \\ \dot{y}_3 = -(\rho_1 y_1 + \rho_2 y_2 + \rho_3) y_3 - \rho_0 y_3^2, \end{cases} \quad (7)$$

with

$$\begin{cases} \rho_3 = \frac{1}{n_3} \sum_{i=1}^3 n_i a_{i3}, & \rho_0 = \sum_{i=1}^3 n_i b_i, \\ \rho_1 = \sum_{i=1}^3 n_i a_{i1} - n_1 \rho_3, & \rho_2 = \sum_{i=1}^3 n_i a_{i2} - n_2 \rho_3. \end{cases} \quad (8)$$

When $n_1 = n_2 = 0$ and $n_3 = 1$, $(\rho_0, \rho_1, \rho_2, \rho_3)$ reduces to $(b_3, a_{31}, a_{32}, a_{33})$. Accordingly, $\dot{y}(t)$ becomes

$$\begin{cases} \dot{y}_1 = a_{13} + (a_{11} - a_{33}) y_1 + a_{12} y_2 - a_{31} y_1^2 \\ \quad - a_{32} y_1 y_2 + (b_1 - b_3 y_1) y_3, \\ \dot{y}_2 = a_{23} + a_{21} y_1 + (a_{22} - a_{33}) y_2 - a_{31} y_1 y_2 \\ \quad - a_{32} y_2^2 + (b_2 - b_3 y_2) y_3, \\ \dot{y}_3 = -(a_{31} y_1 + a_{32} y_2 + a_{33}) y_3 - b_3 y_3^2, \end{cases} \quad (9)$$

which has been presented in [12], [13], [14].

It can be observed that the dynamic system (7) fits into the form of the following nonlinear system:

$$\begin{cases} \dot{x}_1 = w^T(x_1, u) x_2 + \phi(x_1, u), \\ \dot{x}_2 = g(x_1, x_2, u), \\ y = x_1, \end{cases} \quad (10)$$

where the matrix $w^T(x_1, u)$ and the vector $g(x_1, x_2, u)$ are nonlinear functions of their arguments, and where an identifier based observer (IBO) has been proposed for the state estimation [12]. Thus, state estimation of the perspective dynamic system (7) can be carried out using the IBO.

III. PDS WITH BALL-SHAPE IMAGING SURFACES

Consider a spherical imaging surface, shown in Fig. 2, where the center of the sphere and the radius R are assumed to be $[0, 0, 0]^T$ and $R = 1$. Any point $[X_p, Y_p, Z_p]^T$ on the sphere satisfies $X_p^2 + Y_p^2 + Z_p^2 = 1$. We can have $X_p = X/\mathbf{L}_s, Y_p = Y/\mathbf{L}_s, Z_p = Z/\mathbf{L}_s$, where $\mathbf{L}_s \triangleq \sqrt{X^2 + Y^2 + Z^2}$ and the subscript_s denotes the *spherical* imaging surface.

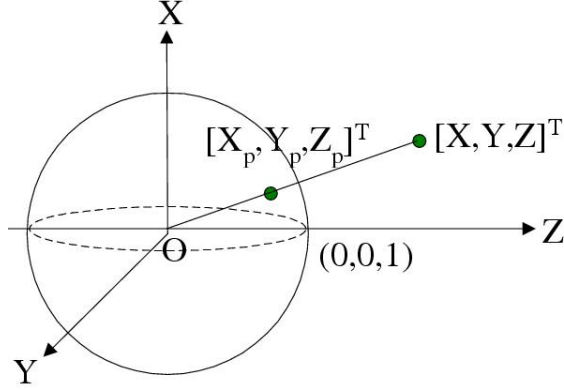


Fig. 2. A spherical imaging surface centered at $[0, 0, 0]^T$ with radius $R = 1$.

A. Range Identification via Spherical Surface

By letting $y(t) = [y_1, y_2, y_3, y_4]^T$ be

$$y_1 = X/\mathbf{L}_s, y_2 = Y/\mathbf{L}_s, y_3 = Z/\mathbf{L}_s, y_4 = 1/\mathbf{L}_s, \quad (11)$$

where (y_1, y_2, y_3) are observable from the imaging surface and y_4 contains the range information to estimate, $[X, Y, Z]^T$ can be calculated as $X = y_1/y_4, Y = y_2/y_4, Z = y_3/y_4$. After some derivations, we can write the derivative of $y(t)$ as:

$$\begin{cases} \dot{y}_k = \sum_{i=1}^3 a_{ki} y_i - y_k f_s(\cdot) + [b_k - y_k g_s(\cdot)] y_4, \\ \dot{y}_4 = -y_4 [f_s(\cdot) + y_4 g_s(\cdot)], \end{cases} \quad (12)$$

for $k = 1, 2, 3$, where

$$\begin{cases} f_s(\cdot) = \sum_{i=1}^3 a_{ii} y_i^2 + \frac{1}{2} \sum_{i,j=1, i \neq j}^3 (a_{ij} + a_{ji}) y_i y_j, \\ g_s(\cdot) = \sum_{i=1}^3 b_i y_i. \end{cases} \quad (13)$$

Equation (12) is again in the form of (10) and the IBO can be applied for the state estimation.

B. Range Identification via Ellipsoid Surface

A spherical imaging surface can be further extended to an ellipsoid, such as characterized by $\frac{X_p^2}{r_1^2} + \frac{Y_p^2}{r_2^2} + \frac{Z_p^2}{r_3^2} = 1$. The projection on the ellipsoid satisfies $X_p = X/\mathbf{L}_e, Y_p = Y/\mathbf{L}_e, Z_p = Z/\mathbf{L}_e$, where $\mathbf{L}_e \triangleq \sqrt{\frac{X^2}{r_1^2} + \frac{Y^2}{r_2^2} + \frac{Z^2}{r_3^2}}$ and the subscript_e denotes the *ellipsoid*. Similar to the case of a spherical imaging surface, $y(t) = [y_1, y_2, y_3, y_4]^T$ can be chosen as $y_1 = X/\mathbf{L}_e, y_2 = Y/\mathbf{L}_e, y_3 = Z/\mathbf{L}_e, y_4 = 1/\mathbf{L}_e$.

After mathematical manipulations similar to those in (12), we can have

$$\begin{cases} \dot{y}_k = \sum_{i=1}^3 a_{ki} y_i - y_k f_e(\cdot) + [b_k - y_k g_e(\cdot)] y_4, \\ \dot{y}_4 = -y_4 [f_e(\cdot) + y_4 g_e(\cdot)], \end{cases} \quad (14)$$

with $k = 1, 2, 3$ and

$$\begin{cases} f_e(\cdot) = \sum_{i=1}^3 \frac{a_{ii}}{r_i^2} y_i^2 + \left(\frac{a_{12}}{r_1^2} + \frac{a_{21}}{r_2^2}\right) y_1 y_2 \\ \quad + \left(\frac{a_{13}}{r_1^2} + \frac{a_{31}}{r_3^2}\right) y_1 y_3 + \left(\frac{a_{23}}{r_2^2} + \frac{a_{32}}{r_3^2}\right) y_2 y_3, \\ g_e(\cdot) = \sum_{i=1}^3 \frac{b_i}{r_i^2} y_i. \end{cases} \quad (15)$$

IV. PDS WITH PARABOLOID IMAGING SURFACE

In this section, we consider a paraboloid imaging surface, as shown in Fig. 3, characterized by $Z_p = X_p^2 + Y_p^2$. A 3D point is projected onto the imaging surface as $X_p = XZ/\mathbf{L}_{pa}, Y_p = YZ/\mathbf{L}_{pa}, Z_p = Z^2/\mathbf{L}_{pa}$, where $\mathbf{L}_{pa} \triangleq X^2 + Y^2$ and the subscript_{pa} denotes the *paraboloid*.

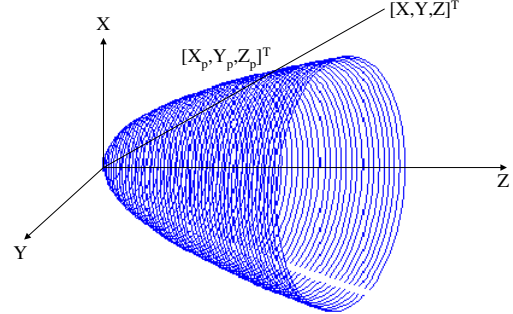


Fig. 3. A paraboloid imaging surface centered at $[0, 0, 0]^T$.

Similarly, the output $y(t)$ can be chosen to be $y(t) = [y_1, y_2, y_3, y_4]^T = [X_p, Y_p, Z_p, 1/\mathbf{L}_{pa}]^T$, where (y_1, y_2, y_3) are observable and y_4 contains the range information to estimate. The procedure to derive $\dot{y}(t)$ is the same as those performed earlier in sections II and IV. However, in the derivations, we need quantities $X/\mathbf{L}_{pa}, Y/\mathbf{L}_{pa}, Z/\mathbf{L}_{pa}$, which are nonlinear functions of y_1, y_2, y_3 , as shown below:

$$\begin{aligned} X/\mathbf{L}_{pa} &= y_1 \sqrt{y_4/y_3}, \\ Y/\mathbf{L}_{pa} &= y_2 \sqrt{y_4/y_3}, \\ Z/\mathbf{L}_{pa} &= \sqrt{y_3 y_4}. \end{aligned} \quad (16)$$

Denote $y_5 = X/\mathbf{L}_{pa}, y_6 = Y/\mathbf{L}_{pa}, y_7 = Z/\mathbf{L}_{pa}$, we have

$$\begin{cases} \dot{y}_1 = \sum_{i=1}^3 a_{1i} y_i + a_{31} \frac{y_1^2}{y_3} + a_{32} \frac{y_1 y_2}{y_3} + a_{33} y_1 - 2y_1 f_{pa}(\cdot) \\ \quad + (b_3 - 2b_1 y_1) y_5 - 2b_2 y_1 y_6 + b_1 y_7, \\ \dot{y}_2 = \sum_{i=1}^3 a_{2i} y_i + a_{31} \frac{y_1 y_2}{y_3} + a_{32} \frac{y_2^2}{y_3} + a_{33} y_2 - 2y_2 f_{pa}(\cdot) \\ \quad - 2b_1 y_2 y_5 + (b_3 - 2b_2 y_2) y_6 + b_2 y_7, \\ \dot{y}_3 = 2 \left[\sum_{i=1}^3 a_{3i} y_i - y_3 f_{pa}(\cdot) - b_1 y_3 y_5 - b_2 y_3 y_6 + b_3 y_7 \right], \\ \dot{y}_4 = -2y_4 [f_{pa}(\cdot) + b_1 y_5 + b_2 y_6], \end{cases} \quad (17)$$

where

$$f_{\text{pa}}(\cdot) = a_{11} \frac{y_1^2}{y_3} + (a_{21} + a_{12}) \frac{y_1 y_2}{y_3} + a_{22} \frac{y_2^2}{y_3} + a_{13} y_1 + a_{23} y_2.$$

In the above derivations, the following entries have been used:

$$\frac{XY}{\mathbf{L}_{\text{pa}}} = \frac{y_1 y_2}{y_3}, \quad \frac{X^2}{\mathbf{L}_{\text{pa}}} = \frac{y_1^2}{y_3}, \quad \frac{Y^2}{\mathbf{L}_{\text{pa}}} = \frac{y_2^2}{y_3}. \quad (18)$$

It can be observed that equation (17) is no longer in the form of (10). Accordingly, the IBO observer can not be applied directly as the other two cases discussed earlier (most of the existing perspective nonlinear observers can not either). For the system (17), the range identification can be performed by using the linear approximation-based observer (LAO), where state estimation of an original nonlinear system is carried out by a sequence of LTV observers [15]. Not surprisingly, the IBO observer can be applied as the individual LTV observer due to the special forms of (10) and (17). Simulation result of the range identification using LAO with IBO inside will be presented in Sec. V.

V. SIMULATION RESULTS

In this section, simulation results are first presented for the range identification with the following four imaging surfaces:

- 1) a traditional camera-type plane.
- 2) a plane passing through $[0, 0, 1]^T$ with $\vec{\mathbf{n}} = [1, 1, 1]^T$.
- 3) a sphere centered at origin with radius 1.
- 4) an ellipsoid centered at origin with $r_1^2 = 1$, $r_2^2 = 2$, and $r_3^2 = 3$.

Among several existing nonlinear observers applicable to the range identification problem, the IBO proposed in [12] is implemented in our simulations due to its easy extension. The perspective observer proposed in [13] can achieve comparable performance to the IBO, and thus the simulation results are not shown here. The range identification observer presented in [14] is more sensitive to noise. The specific affine motion used in our simulation is [13]:

$$\begin{bmatrix} \dot{X}(t) \\ \dot{Y}(t) \\ \dot{Z}(t) \end{bmatrix} = \begin{bmatrix} -0.2 & 0.4 & -0.6 \\ 0.1 & -0.2 & 0.3 \\ 0.3 & -0.4 & 0.4 \end{bmatrix} \begin{bmatrix} X(t) \\ Y(t) \\ Z(t) \end{bmatrix} + \begin{bmatrix} 0.5 \\ 0.25 \\ 0.3 \end{bmatrix}, \quad (19)$$

$$[X(0) \ Y(0) \ Z(0)]^T = [0.4 \ 0.6 \ 1]^T.$$

For a nonlinear system in the form of (10) satisfying the observability condition that for some ε , $\lambda_{\min}\{w w^T\} > \varepsilon$, the IBO observer takes the form:

$$\begin{cases} \dot{\hat{x}}_1 = GA(\hat{x}_1 - x_1) + w^T(x_1, u)\hat{x}_2 + \phi(x_1, u), \\ \dot{\hat{x}}_2 = -G^2 w(x_1, u)P(\hat{x}_1 - x_1) + g(x_1, \hat{x}_2, u), \\ \hat{x}(t_i^+) = M \frac{\hat{x}(t_i^-)}{\|\hat{x}(t_i^-)\|}, \end{cases} \quad (20)$$

with the sequences of t_i defined via

$$t_i = \min \{t : t > t_{i-1} \text{ and } \|\hat{x}(t)\| \geq \gamma M\}, \quad (21)$$

and the matrix P a positive-definite solution of the Lyapunov equation $A^T P + P A = -Q$. The scalar M is an

assumed upper bound for the state estimate $\|\hat{x}(t)\|$ and γ is a fixed constant scalar with $\gamma > 1$. The G in (20) is a constant scalar gain.

Choosing the observer parameters to be $M = 10$, $G = 10$, $\gamma = 1$, state estimation errors for y_3 in (7) and (9), and y_4 in (12) and (14), when using the four surfaces described above are shown in Fig. 4. In the simulations, we apply a relative uniform noise of level 10^{-2} to the system output according to $y(t) = y^*(t) + |y^*(t)| \cdot \text{noise_level} \cdot \text{randn}(\text{length}(y(t)))$, where $y^*(t)$ denotes the ideal system output and $y(t)$ simulates the observed one. $\text{length}(\cdot)$ and $\text{randn}(\cdot)$ are Matlab functions giving the length of a vector and random entries of normal distribution with mean zero, variance one and standard deviation one.

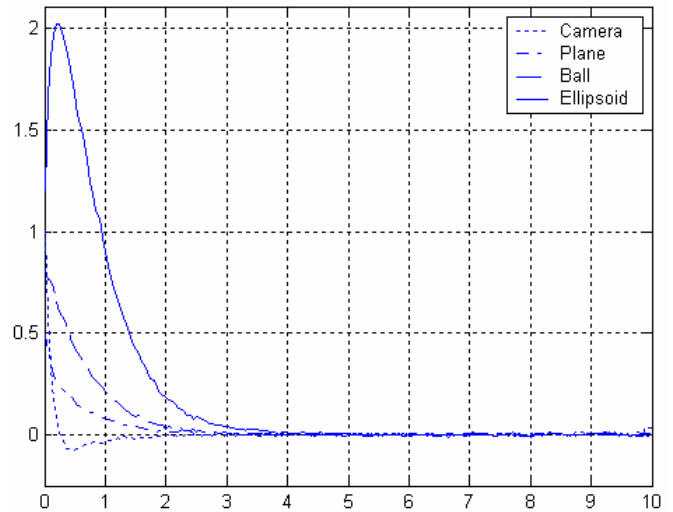


Fig. 4. Range identification error when noise level = 10^{-2} .

For the case of a paraboloid surface, the range identification is performed using the LAO with IBO inside. State estimation error of y_4 in (17) is shown in Fig. 5.

VI. CONCLUDING REMARKS

Range identification problem is discussed on generalized 3D imaging surfaces, such as a plane, a sphere, an ellipsoid, and a paraboloid. We assume that the omnidirectional systems still possess a single center of projection such that the images observed preserve the linear perspective geometry. The underlying nature of the perspective projection is not changed. Furthermore, the basic idea to perform range identification and 3D motion estimation remains the same.

However, different imaging surfaces result in slightly different system structure of the perspective dynamic systems (PDS). When the resulting PDS system no longer preserves an affine form, range identification can not be carried out directly via most of the existing perspective nonlinear observers. In this case, linear approximation-based observer can be applied.

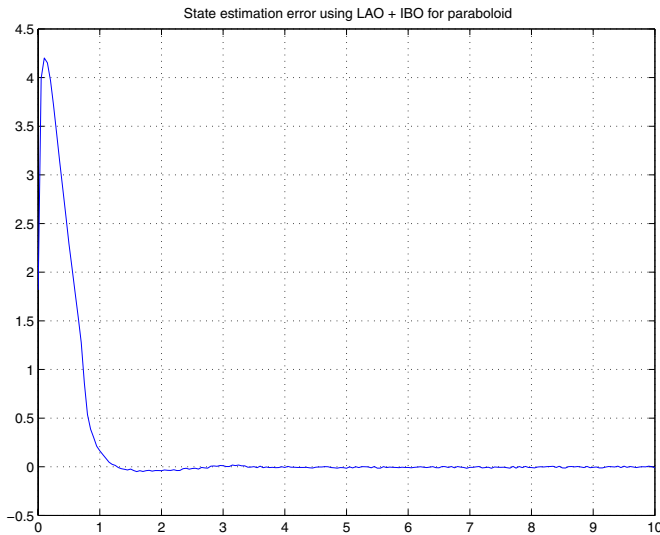


Fig. 5. Range identification error when noise level = 10^{-2} (paraboloid case).

[15] Lili Ma, YangQuan Chen, and Kevin L. Moore, "Range identification for perspective dynamic systems using linear approximation," in *IEEE Int. Conf. on Robotics and Automation*, New Orleans, April 26-May 1 2004.

REFERENCES

- [1] Christopher Geyer and Kostas Daniilidis, "Catadioptric projective geometry," *Int. Journal of Computer Vision*, vol. 45, no. 3, pp. 223–243, 2001.
- [2] Rahul Swaminathan, Michael D. Grossberg, and Shree K. Nayar, "A perspective on distortions," in *IEEE Int. Conf. on Computer Vision and Pattern Recognition*, 2003.
- [3] Shree K. Nayar, "Catadioptric omnidirectional camera," in *IEEE Int. Conf. on Computer Vision and Pattern Recognition*, Puerto Rico, June 1997.
- [4] Lili Ma, *Vision-Based Measurements for Dynamic Systems and Control*, Ph.D. thesis, Utah State University, 2004.
- [5] Bijoy K. Ghosh, Mrdjan Jankovic, and Y. T. Wu, "Perspective problems in system theory and its application to machine vision," *Journal of Mathematical Systems, Estimation and Control*, vol. 4, no. 1, pp. 3–38, 1994.
- [6] B. K. Ghosh and E. P. Loucks, "A perspective theory for motion and shape estimation in machine vision," *SIAM Journal of Control and Optimization*, vol. 35, no. 5, pp. 1530–1559, 1995.
- [7] Bijoy K. Ghosh, Hiroshi Inaba, and Satoru Takahashi, "Identification of Riccati dynamics under perspective and orthographic observations," *IEEE Transactions on Automatic Control*, vol. 45, no. 7, pp. 1267–1278, July 2000.
- [8] Bijoy K. Ghosh and Clyde F. Martin, "Homogeneous dynamical systems theory," *IEEE Transactions on Automatic Control*, vol. 47, no. 3, pp. 462–472, Mar. 2002.
- [9] Satoru Takahashi and Bijoy K. Ghosh, "Motion and shape identification with vision and range," *IEEE Transactions on Automatic Control*, vol. 47, no. 8, pp. 1392–1396, Aug. 2002.
- [10] Stefano Soatto, Ruggero Frezza, and Pietro Perona, "Motion estimation via dynamic vision," *IEEE Transactions on Automatic Control*, vol. 41, no. 3, pp. 393–413, Dec. 1996.
- [11] Joao P. Hespanha, "State estimation and control for systems with perspective outputs," in *Proceedings of the IEEE Conf. on Decision and Control*, Las Vegas, Nevada, USA, Dec. 2002, pp. 2208–2213.
- [12] Mrdjan Jankovic and Bijoy K. Ghosh, "Visually guided ranging from observations of points, lines and curves via an identifier based nonlinear observer," *Systems and Control Letters*, vol. 25, pp. 63–73, 1995.
- [13] Xinkai Chen and Hiroyuki Kano, "A new state observer for perspective systems," *IEEE Transactions on Automatic Control*, vol. 47, no. 4, pp. 658–663, Apr. 2002.
- [14] W. E. Dixon, Y. Fang, D. M. Dawson, and T. J. Flynn, "Range identification for perspective vision systems," *IEEE Transactions on Automatic Control*, vol. 48, no. 12, pp. 2232–2238, 2003.